J. Fluid Mech. (1999), *vol.* 395, *pp.* 295–319. Printed in the United Kingdom

Linear double-diffusive–inertial instability at the equator

By N. R. EDWARDS AND K. J. RICHARDS

Southampton Oceanography Centre, Empress Dock, Southampton SO14 3ZH, UK

(Received 16 November 1998 and in revised form 13 May 1999)

Motivated by observations of interleaving in the equatorial Pacific, we consider the linear stability of a basic state on an equatorial β-plane which is susceptible to both double-diffusive interleaving, driven by a meridional salinity gradient, and inertial instability driven by meridional shear. In a parameter regime compatible with the observations strong interaction can occur between the two processes, indicating that the stability of the system is dependent on the meridional gradients of both salinity and zonal velocity. Meridional shear is found to enhance the interleaving motion even for values of shear well below the cutoff for inertial instability. In the presence of diffusion inertial instability can also be excited by vertical shear, but only if the shear is comparable to the buoyancy frequency. When double-diffusive driving is weak relative to inertial driving the growth can be oscillatory, in which case the mechanism for instability is viscous–diffusive. In this case interleaving layers can slope downwards towards the fresh side of the front in the fingering regime, inhibiting their own growth.

1. Introduction

Accurate prediction of the mean state of the ocean requires a thorough understanding of the effects of small-scale oceanic mixing processes. Indeed, Neelin *et al.* (1992) suggest that deficiencies in the parameterization of subgrid-scale mixing may be largely responsible for the failure of current coupled models to reproduce certain features of the tropical climatology. This problem is particularly acute in the equatorial Pacific, where a highly complicated structure of current and thermohaline fields exists, the detailed dynamics of which are still under debate.

It is generally assumed that the dominant process responsible for oceanic mixing below the grid scale of present models is lateral transport by meso- (100 km) scale eddies, accompanied by effectively vertical mixing due to the turbulent internal wave field on the micro scale of cm to km. However, the widespread occurrence of statically unstable salinity distributions in the oceanic thermocline makes double diffusion another potentially very important agent for micro-scale mixing (see for example the review by Schmitt 1994 and recent work of Zhang, Schmitt & Huang 1998). Double diffusion can also give rise to meso-scale instability in the form of quasi-horizontal interleaving. Banks & Richards (1998) suggest that, in the equatorial Pacific, the transport of tracers due to interleaving may be comparable to that due to the eddy field.

Observations of interleaving in the equatorial Pacific thermocline have been reported by Toole (1981), McPhaden (1985), Richards & Pollard (1991) and by Banks & Richards (1998), who found layers of warm, salty, south Pacific water alternating with cool, fresh layers from the north Pacific, typically 20 m thick and extending for up to 100 km across the equator. Banks & Richards showed that at least 50% of the

observed layers had properties consistent with the hypothesis of a double-diffusive driving mechanism, and that layering was strongest when the cross-equatorial salinity gradient was strongest. Banks & Richards concluded that double diffusion was likely to be important in the formation and maintenance of the layers, but other processes cannot be excluded. In particular inertial instability, often referred to as symmetric instability by the atmospheric community, has been put forward by Hua, Moore & Le Gentil (1997) as a possible explanation for the equatorial deep jets observed in all three equatorial oceans, and this process may also play an important role within the thermocline. Both double-diffusive and inertial instability correspond to linear instabilities of the background flow. Woods, Onken & Fischer (1986) have shown that differential advection by the essentially nonlinear, meso-scale eddy field can produce layers with cross-isopycnal slopes similar to those characteristic of double-diffusive interleaving.

In this paper we concentrate on the linear theory of meso-scale interleaving produced by double-diffusive and inertial instability and address the question of their relative importance by analysing a model in which both mechanisms are active. The linear theory of double-diffusive interleaving originated with Stern (1967) and was developed by Toole & Georgi (1981) and McDougall (1985) to include the effects of rotation and different vertical mixing schemes. Richards (1991) extended the linear theory to the equatorial β-plane and found that the variation in Coriolis parameter controls the latitudinal extent of the layers and gives rise to weak zonal jets. The theory of inertial instability goes back to Rayleigh (1916), who derived the stability criterion for an inviscid circular vortex. Equatorial inertial instability has been studied by Dunkerton (1981, 1983) and by Hua *et al.* (1997), who include the full Earth rotation vector in their linear analysis, and go on to study the nonlinear equilibriation of linearly unstable disturbances. May & Kelley (1997) have investigated the effect of baroclinic shear on double-diffusive interleaving for the case of constant Coriolis parameter f, but inertial instability driven by horizontal shear is not considered in their analysis.

The present work considers the situation when both double-diffusive and inertial instability can occur on an equatorial β-plane. Due to variation of the Coriolis parameter, the equator is a preferred location for symmetric inertial instability, which acts to redistribute angular momentum via a system of zonal jets. Zonally symmetric double-diffusive interleaving modes at the equator can also have significant growth rates, and also give rise to a system of zonal jets. Hence, by considering an equatorial β-plane, we have the interesting possibility of interaction between inertial and double-diffusive instabilities.

We present an analysis of an idealized system in which both double-diffusive and inertial instability can occur. To aid qualitative understanding we make a number of simplifying assumptions which allow us to obtain solutions which can be expressed in closed form. First of all, following Stern (1967), we assume that there is a three-way scale separation between the micro-scale mixing, meso-scale interleaving, and the large-scale background (or mean) flow. We assume the background gradients are such that we can take the micro-scale mixing to be dominated by double-diffusive convection, which we parameterize as a simple diffusive process in which the vertical fluxes of heat and salt are in a constant ratio, as found in the laboratory study of Turner (1967). The large-scale flow is a geostrophically balanced zonal flow which is sheared in either the meridional or vertical direction. Perturbations about the mean state are assumed to vary only in the meridional and vertical directions. This system is sufficient to demonstrate that there can be a strong interaction between inertial and double-diffusive instabilities in a parameter regime compatible with the equatorial Pacific. The underlying assumptions, in particular the restriction to two dimensions, will be discussed in § 8.

In the next Section we present the model problem and governing linear equations. The mechanisms for instability are described in § 3, and the next four Sections then consider a heirarchy of increasingly general sub-problems, starting with the inviscid case in § 3. Conclusions are presented in § 8.

2. Governing equations

We consider the linear stability of a basic state which is potentially susceptible to both inertial instability and double-diffusive interleaving. To drive inertial instability we allow for a zonal mean flow $\bar{u}$ which varies linearly with y, the meridional coordinate, and z, the vertical coordinate, so that $\bar{u} = 2\Lambda y + Gz$, where Λ and G are constants. The mean salinity field $\bar{S}$ is also assumed to depend linearly on y and z so that its meridional and vertical gradients, denoted $\bar{S}_y$ and $\bar{S}_z$ respectively, are constant. We assume that the mean vertical gradients of salinity S and temperature T are favourable to double-diffusive convection, which we parameterize in the equation for salinity in terms of a constant vertical diffusivity A. Diffusive fluxes of heat and salt are then assumed to be in a constant ratio γ. The flux ratio γ is less than one for fingering and greater than one for diffusive layering. For analytical tractability we restrict the problem to two dimensions by neglecting variations in the zonal direction. Under these assumptions the linearized governing equations for small perturbations about the mean state are

$$\left.\begin{gathered} u'_t + (2\Lambda - f)v' + Gw' = \nu u'_{zz}, \quad v'_t + fu' + \rho_0^{-1}p'_y = \nu v'_{zz}, \\ w'_t + g\rho_0^{-1}\rho' + \rho_0^{-1}p'_z = \nu w'_{zz}, \\ v'_y + w'_z = 0, \\ S'_t + v'\bar{S}_y + w'\bar{S}_z = AS'_{zz}, \quad T'_t + v'\bar{T}_y + w'\bar{T}_z = \gamma\delta\alpha^{-1}AS'_{zz}, \end{gathered}\right\} \tag{2.1}$$

and the linearized equation of state is

$$\rho' = \rho_0(\delta S' - \alpha T'), \tag{2.2}$$

where u, v, and w are the velocity components in a right-handed coordinate system (x, y, z) on an equatorial β-plane with x directed eastward (thus the Coriolis parameter $f = \beta y$, and the equator is located at $y = 0$); α and δ are the thermal expansion and saline contraction coefficients, which are assumed to be constant. An overbar denotes the mean state and perturbations to this state are denoted by a prime. ρ_0 is a constant reference density and p is the pressure. The viscosity ν is also assumed to be constant. Since the mean flow will be assumed to obey the thermal wind equations, we must have $g\bar{\rho}_y = Gf\rho_0$. The buoyancy frequency N, defined by $N^2 = -g\bar{\rho}_z/\rho_0$, is assumed to be constant.

We look for harmonic solutions to (2.1) so that, for instance, $v = \hat{v}(y)e^{\lambda t + imz}$. After some algebra we find that $\hat{v}$ obeys

$$a\hat{v}_{yy} + b\hat{v}_y + c(y)\hat{v} = 0, \tag{2.3}$$

where

$$\left.\begin{gathered} a = \lambda + Am^2(1 + \epsilon_z) + \frac{\lambda\lambda_A\lambda_\nu}{N^2}, \\ b = b_0 + 2b_1 y, \quad b_0 = -iAm^3\epsilon_y, \quad b_1 = \frac{imG\beta\lambda_A}{2\lambda_\nu N^2}(\lambda + \lambda_\nu), \\ c = -\frac{m^2}{N^2}\frac{\lambda}{\lambda_\nu}\lambda_A(\lambda_\nu^2 + \beta y(\beta y - \bar{u}_y)) + \frac{i\beta Gm\lambda_A}{N^2}, \\ \lambda_A = \lambda + Am^2, \quad \lambda_\nu = \lambda + \nu m^2, \end{gathered}\right\} \tag{2.4}$$

and ϵ_y and ϵ_z are dimensionless measures of the strength of the salinity gradients relative to the density stratification. They are thus defined by

$$\epsilon_y = \frac{(1-\gamma)g\delta\bar{S}_y}{N^2}, \qquad \epsilon_z = \frac{(1-\gamma)g\delta\bar{S}_z}{N^2}. \tag{2.5}$$

To solve (2.3) we transform to a parabolic vertical coordinate

$$z^* = z - \frac{b_1}{2aim}y^2 - \frac{b_0}{2aim}y. \tag{2.6}$$

Hua *et al.* (1997) use a similar transformation in the ideal fluid case, interpreting the parabolic coordinates as surfaces of absolute angular momentum. Solutions remain harmonic with respect to the transformed vertical coordinate, and straightforward manipulation of (2.3) shows that such solutions can be expressed in terms of parabolic cylinder functions. Our interest is in equatorially trapped solutions which decay in the limit $y \to \pm\infty$. This boundary condition results in an eigenvalue problem with solutions of the form

$$\hat{v}(y) = H_n(\eta)\mathrm{e}^{-\eta^2/2+\mathrm{i}ly}, \tag{2.7}$$

where H_n is the nth-order Hermite polynomial (Jeffreys & Jeffreys 1956) and η and l are given by

$$\eta = C\beta(y - y_0), \quad l = \frac{\mathrm{i}}{2a}(b_0 + b_1 y), \tag{2.8}$$

where

$$C^4 = \left(\frac{m}{\beta N}\right)^2 \frac{\lambda\lambda_A}{a\lambda_v} + \left(\frac{b_1}{a\beta^2}\right)^2, \quad y_0 = \frac{4a\lambda\lambda_v\Lambda - Am^2\lambda_v\epsilon_y G(\lambda+\lambda_v)}{4a\beta\lambda_v\lambda - \lambda_A\beta(G/N)^2(\lambda+\lambda_v)^2}. \tag{2.9}$$

The eigenvalues λ satisfy the dispersion relation

$$C^4\beta^2 y_0^2 - \frac{\lambda_A}{a}\left(\frac{m}{\beta N}\right)^2\left(\lambda\lambda_v - \frac{\mathrm{i}mvG\beta}{2\lambda_v}\right) - \left(\frac{b_0}{2a\beta}\right)^2 = (2n+1)C^2, \tag{2.10}$$

where n corresponds to the order of the Hermite polynomial. By squaring both sides of (2.10), we obtain a dispersion relation $D(\lambda) = 0$ for λ, which could, in principle, be expressed in the form of a polynomial of order 20 with complex coefficients. Evaluating the coefficients of the polynomial in the form of a power series is impractical. Therefore we solve for λ directly with a standard library routine which combines Newton and gradient search methods. Our algorithm iteratively searches for the 20 roots to the equation $D(\lambda) = 0$, dividing D by $(\lambda - \lambda_i)$ each time the library root-finding routine finds a root or a numerical singularity λ_i. We must discard any unphysical roots which correspond to negative C^2 and hence grow exponentially away from the equator, thus violating the assumptions used to derive the eigenvalue condition. Note that it is not obvious on purely mathematical grounds how many roots have $C^2 < 0$. However, comparison with the constant-f problem suggests that there may be only four roots which represent distinct physical solutions. In practice we will usually only be concerned with the solutions which have the largest real growth rate for a given set of parameters, since these are the solutions most likely to be observed in practice. In all cases studied here the largest growth rates are associated with the gravest lateral mode, $n = 0$ in (2.7), corresponding to the zeroth-order Hermite polynomial $H_0 \equiv 1$. To locate the most unstable mode we search for all the solutions at a given vertical wavenumber m, then repeat the entire process for a range of equally spaced values of m. Close inspection shows that the

dispersion relation (2.10), and hence the growth rate of the instability, depends only on the square of the latitudinal salinity gradient. If $G = 0$ then only the square of mean shear Λ is involved, while if $\Lambda = 0$ then changing the sign of G corresponds to interchanging m and $-m$, or taking the complex conjugate, and hence does not affect the real part of the growth rate. Therefore we need only consider a single sign of shear or salinity gradient, as long as $\Lambda G = 0$.

Note that we can trivially recover the mid-latitude f-plane problem by replacing y-derivatives in (2.3) by i times a northward wavenumber. We then obtain a polynomial of only fourth order in the growth rate λ, which gives the instability criterion derived by May & Kelley (1997).

The dimensional problem depends on the ten physical parameters A, ν, γ, β, $\overline{\rho}_y$, $\overline{\rho}_z$, $\overline{S}_y$, $\overline{S}_z$, $\overline{u}_y$ and $\overline{u}_z$. In principle we could remove the physical dimensions of time and length from this set, for instance by scaling with N and $(A/N)^{1/2}$, leaving a set of eight dimensionless parameters. One of these is redundant because the mean flow is assumed to obey the thermal wind relation between $\overline{u}_z$ and $\overline{\rho}_y$. Further the flux ratio γ and the mean salinity gradients are not all independent, since γ does not appear explicitly in the solution if these three variables are combined into the two dimensionless salinity gradients ϵ_z and ϵ_y. Thus the results of the analysis can be described by a set of six independent dimensionless parameters. If we choose to represent the strengths of viscosity and rotation by the parameters

$$\sigma = \nu/A \quad \text{and} \quad s = \beta^2 A/N^3, \tag{2.11}$$

the first of which is a Schmidt number, then the mean gradients of density, salinity and velocity can be described by the four independent dimensionless parameters

$$\epsilon_z, \quad \epsilon_y, \quad \Lambda/N \quad \text{and} \quad G/N. \tag{2.12}$$

For the present study we will keep the Schmidt number and rotation parameter constant and focus on the effects of varying the mean gradients. For the purposes of illustration we continue to express results in terms of dimensional quantities, taking the buoyancy frequency $N = 0.02\,\mathrm{s}^{-1}$. The diffusivity A is set to $3 \times 10^{-5}\,\mathrm{m}^2\,\mathrm{s}^{-1}$ so that $s = 1.96 \times 10^{-21}$ and the Schmidt number $\sigma = 1$ (or 0 in the inviscid case considered below). We take the thermal expansion and saline contraction coefficients to be $0.17/\rho_0\ \mathrm{K}^{-1}$ and $0.78/\rho_0\,\mathrm{p.s.u.}^{-1}$ (where p.s.u. denotes practical salinity unit) respectively, with $\rho_0 = 1020\,\mathrm{kg\,m}^{-3}$, $g = 9.78\,\mathrm{m\,s}^{-2}$ and the flux ratio $\gamma = 0.5$, which is appropriate to the fingering regime where $\overline{S}_y > 0$.

3. Mechanisms for instability

Inertial instability can be viewed as a response to an unstable distribution of angular momentum, hence the instability is most easily explained in terms of the total angular momentum, which in our system of equations is given by

$$M = u - \tfrac{1}{2}\beta y^2.$$

In terms of M and the zonal vorticity $\zeta = w_y - v_z$, the dynamics in our linearized system are governed by the two equations

$$M'_t + v'\overline{M}_y + w'\overline{M}_z = \nu M'_{zz}, \tag{3.1}$$

$$\zeta'_t + (g/\rho_0)\rho'_y - f M'_z = \nu \zeta'_{zz}, \tag{3.2}$$

along with the temperature, salinity and density equations given in (2.1).

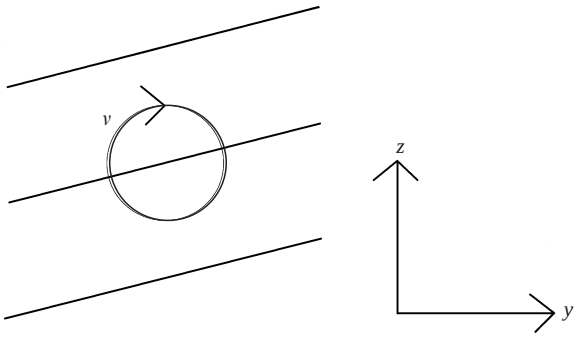

FIGURE 1. Schematic for the explanation of interleaving instability. The sloping lines represent phase lines of perturbations of salinity or angular momentum, the circle represents the resulting vorticity tendency; see text.

The mechanism for double-diffusive interleaving on a wide front can be explained by reference to figure 1. Given a salinity perturbation which is positive in the upper of the two layers shown, and assuming that $\bar{S}_z$, $\bar{T}_z > 0$ so that $\gamma < 1$, the resulting effect of the double-diffusive fluxes will be to create a density perturbation which has the opposite sign, that is negative in the upper layer and positive in the lower layer. If the layer slope is positive, then this results in a negative vorticity tendency at the interface, as shown. This leads to an advection along the layers which can reinforce the initial salinity perturbation if the mean salinity gradient $\bar{S}_y$ is negative. Hence instability is possible if the layers slope upwards towards the fresher water.

The mechanism for inertial instability can be explained by reference to the same picture. Suppose $\bar{u}_y > 0$, then there will be a region in $y > 0$ where both f and $\bar{M}_y$ are positive. This is the unstable region. Now imagine a displacement towards the right in the upper layer and towards the left in the lower layer, within the unstable region. This leads to a negative value of M'_z at the interface and hence a negative vorticity tendency. The resulting along-layer advection of mean angular momentum is such as to reinforce the original disturbance, and instability results. The gravitational torque in the vorticity equation is normally a restoring force; in the absence of angular momentum effects this term is responsible for internal gravity waves.

A third class of instability which is possible in our system relies on the differential diffusion of momentum and density (McIntyre 1970). This instability can be oscillatory owing to a phase shift effect which results in the gravitational restoring force being too strong (McIntyre 1970).

4. Inviscid solutions

Since the general solution given above is somewhat complicated, we will restrict our discussion initially to the simplest sub-class of solutions in which double-diffusive and inertial instability are both active. In this Section we will consider inviscid, hydrostatic solutions with latitudinal mean shear, but no vertical mean shear. In this case the coefficients in (2.3) simplify to

$$a = \lambda + Am^2(1+\epsilon_z), \quad b = -\mathrm{i}Am^3\epsilon_y, \quad c = -\frac{m^2}{N^2}\lambda_A(\lambda^2 + f(f-\bar{u}_y)). \tag{4.1}$$

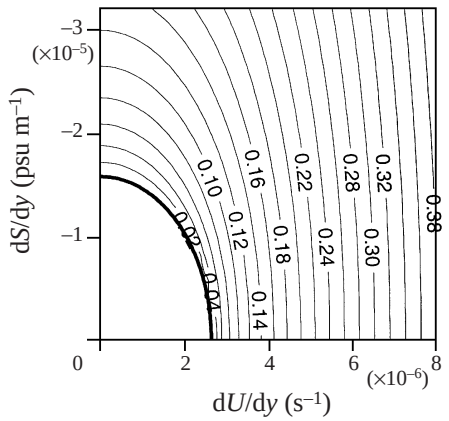

FIGURE 2. Growth rate of the most unstable inviscid mode in units of $10^{-5}\,\mathrm{s}^{-1}$ as a function of latitudinal shear 2Λ and latitudinal salinity gradient $\bar{S}_y$ at $m = 0.3\,\mathrm{m}^{-1}$. Other parameters are $\bar{S}_z = 3 \times 10^{-2}$ p.s.u. m^{-1}, $N = 0.02\,\mathrm{s}^{-1}$. The neutral curve for $\bar{S}_z = 0$ (4.6) is drawn bold. Note from (4.6) that the existence of a stable region is a result of fixing m.

The form of the solution is as given above in (2.7), but the formula for C^4 simplifies to

$$C^4 = \left(\frac{m}{\beta N}\right)^2 \frac{\lambda_A}{a} \tag{4.2}$$

and the equatorial offset becomes $y_0 = \Lambda/\beta$. The dispersion relation (2.10) simplifies to

$$C^4(\Lambda^2 - \lambda^2) - \left(\frac{b}{2a\beta}\right)^2 = (2n+1)C^2 \tag{4.3}$$

which, after squaring both sides and substituting for C^4 to obtain the polynomial form, is only eighth order in λ and the coefficients, which are all real, can be straightforwardly calculated. Having obtained the coefficients we can then find all eight eigensolutions to the problem using a library root-finding routine which is specifically tailored for real polynomials. As described above we discard any unphysical roots.

Apart from our inclusion of shear and neglect of non-hydrostatic effects, and the use of Laplacian diffusion as opposed to the form suggested by McDougall (1985), our solution corresponds to the special case of no zonal variation in the solution found by Richards (1991). Richards found reasonable agreement with observations for vertical wavelength, cross-isopycnal slope, and horizontal extent of interleaving.

In the limit of small A and non-zero $\bar{u}_y$, that is with shear but without double diffusion, the solution collapses to the inviscid solution for inertial instability given by Dunkerton (1981). In this case the solution is displaced from the equator by a distance Λ/β but the northward layer slope is zero.

Figure 2 shows the growth rate of the most unstable double-diffusive–inertial instability mode as a function of latitudinal shear 2Λ and latitudinal salinity gradient $\bar{S}_y$ at $m = 0.3\,\mathrm{m}^{-1}$. Other parameters are $\bar{S}_z = 3 \times 10^{-2}$ p.s.u. m^{-1}, $N = 0.02\,\mathrm{s}^{-1}$. Note that the dispersion relation, and hence the growth rate of the instability, is independent of the signs of mean shear and latitudinal salinity gradient, since only Λ^2 and $\bar{S}_y^2$ appear in (4.3). The sign of Λ determines the sign of the equatorial offset, and the sign of $\bar{S}_y$ determines the sign of the layer slope. At $\bar{S}_y = 0$, instability only occurs

for values of latitudinal shear greater than a certain critical value S_c, which can be found from (4.3) to be $2(\beta N/m)^{1/2}$. For the parameters of figure 2, $S_c = 2.47 \times 10^{-6}\,\mathrm{s}^{-1}$. It is evident from figure 2 that the presence of latitudinal shear modifies the growth rate of the instability even for values of shear well below the inviscid cutoff value S_c. By calculating the change in growth rate with Λ^2 we can show that the growth rate of unstable double-diffusive modes is enhanced by small latidudinal shear, at least if $\epsilon_z = 0$, since, using the dispersion relation and setting $\Lambda = 0$, we find that

$$\frac{\partial \lambda}{\partial(\Lambda^2)} = \frac{a}{2(a\lambda + \lambda^2 + (2n+1)\beta N/m)}. \tag{4.4}$$

Since the right-hand side of this expression is positive, the growth rate is enhanced. Similarly the growth of inertial modes is enhanced by small values of salinity gradient, at least if $\epsilon_z = 0$, since

$$\frac{\partial \lambda}{\partial(\epsilon_y^2)} = \frac{A^2 m^4 N^2}{8\lambda a^2} > 0 \tag{4.5}$$

at $\epsilon_y = 0$. By setting the growth rate to zero in the dispersion relation (4.3) we obtain the equation

$$\Lambda^2 + \frac{N^2}{4(1+\epsilon_z)}\epsilon_y^2 = (2n+1)\frac{\beta N}{m}(1+\epsilon_z)^{1/2} \tag{4.6}$$

for the neutral curve, which describes an ellipse in $\Lambda, \bar{S}_y$ space. The neutral curve is indicated in figure 2. Note that instability is possible for all values of shear and salinity gradient for sufficiently large vertical wavenumber m.

In the unstable region significant growth rates are obtained, which are purely real, hence in this simplified model the most unstable modes grow in place, as in the case of classical symmetric inertial instability. Most importantly, it is evident from the figure that there is significant interaction between shear and double-diffusive modes of instability in this range of parameters.

We can derive an upper bound for the inviscid growth rate using the dispersion relation, which can be written as

$$\Lambda^2 - \lambda^2 + \frac{A^2 m^4 \epsilon_y^2 N^2}{4a^2}\left(\frac{a}{\lambda_A}\right) = (2n+1)\frac{\beta N}{m}\left(\frac{a}{\lambda_A}\right)^{1/2}. \tag{4.7}$$

Therefore, since $a > \lambda_A > \lambda$,

$$\lambda^2 - \frac{A^2 m^4 \epsilon_y^2 N^2}{4\lambda^2} + (2n+1)\frac{\beta N}{m} - \Lambda^2 < 0. \tag{4.8}$$

Since the left-hand side of this inequality is an increasing function of λ for $\lambda > 0$, λ must be bounded above by the unique positive root of the expression on the left-hand side. Hence

$$\lambda < \left(\frac{I^2 + (I^4 + 4D^4)^{1/2}}{2}\right)^{1/2} \tag{4.9}$$

where I and D denote the inertial and double-diffusive parts given by

$$I^2 = \Lambda^2 - (2n+1)\frac{\beta N}{m}, \tag{4.10}$$

$$D^2 = \tfrac{1}{2}\epsilon_y N A m^2. \tag{4.11}$$

The growth rate bound (4.9) is achieved in the inertial limit but overestimates growth rates in the double-diffusive limit by a factor of 2 to 3, hence it may only be useful

as an order of magnitude estimate. On the other hand if we set m to the most unstable wavenumber derived by Toole & Georgi (1981) for the case of constant f and non-zero Schmidt number σ, then for $\Lambda = 0$ we obtain

$$\lambda < \frac{\epsilon_y N}{2\sqrt{2\sigma^{1/4}}}. \tag{4.12}$$

Comparing this estimate with the corresponding value for the maximum growth rate given by McDougall (1985), who found $\lambda = \epsilon_y N/(4\sigma^{1/2})$, suggests that the validity of (4.9) may depend on the appropriate value for σ in double-diffusive convection. Ruddick (1985) gives $\sigma = 40$. However more recent thinking suggests the value may be closer to 1 (Ruddick, Griffiths & Symonds 1989; Kunze 1990).

5. Solutions with viscosity

For the inviscid solutions discussed in the previous Section, the maximum growth rate of the most unstable mode increases indefinitely with wavenumber m. To predict the most unstable vertical wavenumber it is necessary to allow for non-zero viscosity ν in (2.1). Retaining the hydrostatic assumption, and the assumption of zero mean vertical shear, but allowing for non-zero ν, we find that the form of the solution is as given above in (2.7) with the equatorial offset $y_0 = \Lambda/\beta$ and

$$C^4 = \left(\frac{m}{\beta N}\right)^2 \frac{\lambda\lambda_A}{a\lambda_\nu}, \tag{5.1}$$

which is the inviscid relationship for C^4 (4.2) multiplied by $\lambda/(\lambda + \nu m^2)$. Inclusion of viscosity alters the dispersion relation slightly to

$$C^4(\Lambda^2 - \lambda_\nu^2) - \left(\frac{b}{2a\beta}\right)^2 = (2n+1)C^2 \tag{5.2}$$

and increases the amount of algebra required to obtain the coefficients in the squared, polynomial form, but we can still use the same solution method as in the inviscid case. To locate the most unstable mode we search for all the solutions at a given vertical wavenumber m, then repeat the entire process for a range of equally spaced values of m. As in the inviscid case, the dispersion relation, and hence the growth rate of the instability, is independent of the signs of mean shear and latitudinal salinity gradient.

5.1. *Results*

Figure 3 shows the real and imaginary parts of the growth rate of the most unstable mode, and the corresponding wavenumber, as a function of latitudinal shear 2Λ and latitudinal salinity gradient $\bar{S}_y$. Other parameters are $\bar{S}_z = 3 \times 10^{-2}$ p.s.u. m^{-1}, $G = 0$, $N = 0.02\,\mathrm{s}^{-1}$.

Comparing figures 2 and 3, we see that viscosity leads to a reduction in growth rate. Significant interaction between inertial and double-diffusive instability modes is apparent with or without viscosity, albeit shifted slightly towards larger values of shear when viscosity is included. The principal effect of the addition of viscosity is the appearence of a sharply defined transitional region, between diffusive and shear-dominated instability, at small absolute values of salinity gradient. Consultation of figure 3 shows that this is a region of oscillatory instability ($\mathrm{Im}(\lambda) \neq 0$). This oscillatory region persists even when $\bar{S}_y = \bar{S}_z = 0$, at which point our system of

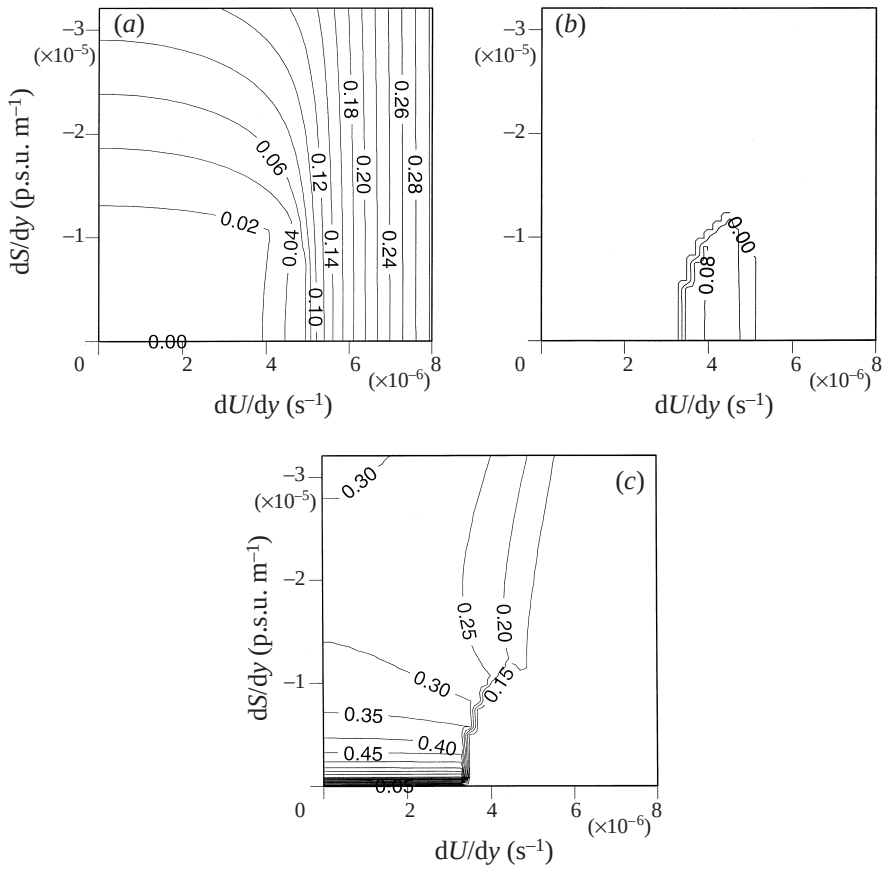

FIGURE 3. (*a*) Real and (*b*) imaginary parts of the growth rate of the most unstable viscous mode in units of $10^{-5}\,\mathrm{s}^{-1}$ as a function of latitudinal shear 2Λ and latitudinal salinity gradient $\bar{S}_y$. (*c*) Corresponding most unstable wavenumber in m^{-1}. Other parameters are $\bar{S}_z = 3 \times 10^{-2}$ p.s.u. m^{-1}, $G = 0$, $N = 0.02\,\mathrm{s}^{-1}$.

equations collapses to one where salinity and temperature, and hence density, are passively advected. Hence the oscillatory instability does not rely on double diffusion. On the other hand, when $\gamma = \alpha = 0$, which implies $\epsilon_y = 1 + \epsilon_z = 0$, our system is equivalent to one with a single active tracer, and σ becomes a Prandtl number. In this case the oscillatory region persists when $\sigma \neq 1$ but vanishes for $\sigma = 1$. Therefore the oscillatory behaviour can be attributed to the differential diffusion of density and momentum, as discussed by McIntyre (1970). Rates of oscillation are significant, the real and imaginary parts of the growth rate in the oscillatory region being of comparable magnitude. It should be noted that Richards (1991) shows that, when zonal variation is included, the growth rate of the most unstable modes can be complex, even in the absence of mean shear.

For the double diffusion-driven modes, the most unstable wavenumber m_c increases with $|\bar{S}_y|$ for large $|\bar{S}_y|$, as found by Toole & Georgi (1981), and also shows a sharp increase as $|\bar{S}_y|$ decreases towards zero, although the growth rates for small absolute values of salinity gradient are very small. For the shear-driven modes m_c decreases as the shear increases. Throughout most of the parameter regime plotted, however, m_c varies by only a factor of 3 or 4, being around $0.3\,\mathrm{m}^{-1}$ where double diffusion is

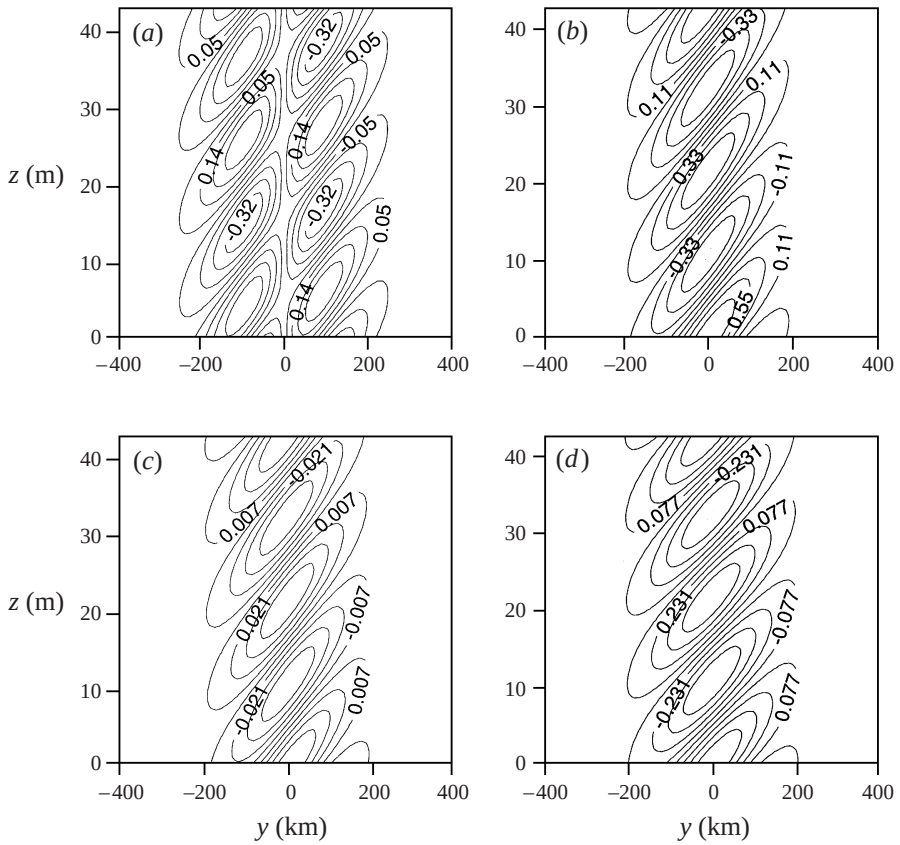

FIGURE 4. Most unstable double-diffusion mode with zero shear for $\bar{S}_y = -2 \times 10^{-5}$ p.s.u. m^{-1}, $\bar{S}_z = 3 \times 10^{-2}$ p.s.u. m^{-1}, $A = G = 0$, $N = 0.02\,\mathrm{s}^{-1}$, (*a*) u' (cm s^{-1}), (*b*) v' (cm s^{-1}), (*c*) S' (p.s.u.) (*d*) T' (K).

dominant, and around 0.1 to 0.15 m^{-1} in the shear-dominated regions, including the oscillatory regime.

The spatial structure of a pure double-diffusion mode is shown in figure 4. The figure shows the perturbation fields of along-front velocity u, across-front velocity v, salinity S and temperature T, for the most unstable mode, at a salinity gradient of $\bar{S}_y = -2 \times 10^{-5}$ p.s.u. m^{-1}, with $\bar{S}_z = 3 \times 10^{-2}$ p.s.u. m^{-1} and $N = 0.02\,\mathrm{s}^{-1}$. The growth rate in this case is $0.45 \times 10^{-6}\,\mathrm{s}^{-1}$, which gives an e-folding time of 26 days, and the most unstable vertical wavelength is 21 m. For this and subsequent figures we arbitrarily set the northward velocity amplitude to 1 cm s^{-1}. As expected, the disturbance takes the form of thermohaline intrusions sloping upwards from warm salty water on the left of the figure, towards cooler, fresher water on the right. As discussed by Richards (1991), the β-effect causes the perturbations to be trapped near the equator, even though the mean thermohaline 'front' is assumed to be uniform and infinite in extent. The meridional trapping scale can be found from (2.7), (2.8) and (5.1) to be $(\mathrm{Re}\,(0.5C^2\beta^2))^{-1/2}$. In this case the trapping scale is approximately $(\beta m/N)^{-1/2}$, which is closely related to the equatorial radius of deformation $(Nh/\beta)^{1/2}$, with the vertical scale $1/m$ taking the place of the layer depth h. An estimate of the meridional displacements required to produce the disturbance shown in figure 4 can be obtained by comparing the rate of change and meridional advection terms in the

salinity equation (2.1). The ratio of these two terms is

$$r = \frac{S'_t}{v'\bar{S}_y} = \frac{\lambda}{\lambda_A}\left(1 + \frac{\hat{w}\bar{S}_z}{\hat{v}\bar{S}_y}\right). \tag{5.3}$$

At the centre of the disturbance, where $\eta = 0$,

$$r = \frac{\lambda}{\lambda_A}\frac{\lambda + Am^2(1+\epsilon_z/2)}{\lambda + Am^2(1+\epsilon_z)}. \tag{5.4}$$

Integrating from some initial time t_0 when the disturbance was small, to a time t, the resulting change in S' is given by

$$\Delta S' = r\bar{S}_y \int_{t_0}^{t} v' \,\mathrm{d}t = r\Delta y \bar{S}_y \tag{5.5}$$

where Δy is the integral of v' at constant y. Since $\epsilon_z \approx 0.3$; $r \approx \lambda/\lambda_A \approx \frac{1}{6}$ in this case. Hence at the centre of the disturbance where $\Delta S' \approx 0.06$ p.s.u., $\Delta y \approx 18$ km. This is not a Lagrangian displacement, but since the velocity changes little over a distance of 18 km in the centre of the disturbance, it is a reasonable estimate for the maximum meridional particle displacement required to produce the disturbance plotted. Also shown in figure 4 is the system of zonal jets which is produced. These jets are a consequence of the meridional variation of the background potential vorticity, and are absent in the constant-f solutions of McDougall (1985). The entire solution is centred on the equator $y = 0$.

Figure 5 shows the spatial structure of the most unstable mode for a latitudinal shear of $\Lambda = 2 \times 10^{-6}\,\mathrm{s}^{-1}$, with other parameters the same as figure 4. The growth rate in this case is $0.65 \times 10^{-6}\,\mathrm{s}^{-1}$, which gives an e-folding time of 18 days, and the most unstable vertical wavelength is 28 m. This is outside the oscillatory regime seen in figure 3, but we expect the solution to be influenced both by double diffusion and by inertial effects. The slope of the layers is visibly reduced by the addition of mean shear, but more striking is the displacement of the centre of the disturbance away from the equator. From (2.7) we expect the displacement to be given by Λ/β which equals 87 km in this case. For the system of zonal jets the effect of shear is more complicated, but readily explained by reference to the zonal momentum equation in (2.1), which reduces to

$$\hat{u} = (\beta y - 2\Lambda)\hat{v}/\lambda_v. \tag{5.6}$$

Linear variation with y of the ratio of $\hat{u}$ and $\hat{v}$ explains the differences between the two fields. Note that an equatorial offset also occurs in the absence of mean shear when zonal variation is included (Richards 1991). Zonal variation also distorts the zonal velocity field since this leads to a term proportional to $\hat{\rho}$ on the right-hand side of (5.6).

To assess the relative contributions of inertial and diffusive effects we consider the vertically integrated kinetic energy equation for the disturbance. The energy equation, which can easily be derived from (2.1), takes the form

$$\frac{1}{2}\frac{\partial}{\partial t}\overline{u'^2 + v'^2} = -2\Lambda\overline{u'v'} - \frac{g}{\rho_0}\overline{\rho' w'} - \nu m^2(u'^2 + v'^2) - \frac{\partial}{\partial y}\overline{p'v'}, \tag{5.7}$$

where the overbar denotes the average over one vertical wavelength, and the primes denote the (real) disturbance quantities. Figure 6 is a plot of terms in (5.7) for the disturbance shown in figure 5. The rate of change of kinetic energy is denoted K in the figure, and the four contributory terms on the right-hand side of (5.7) are, in order:

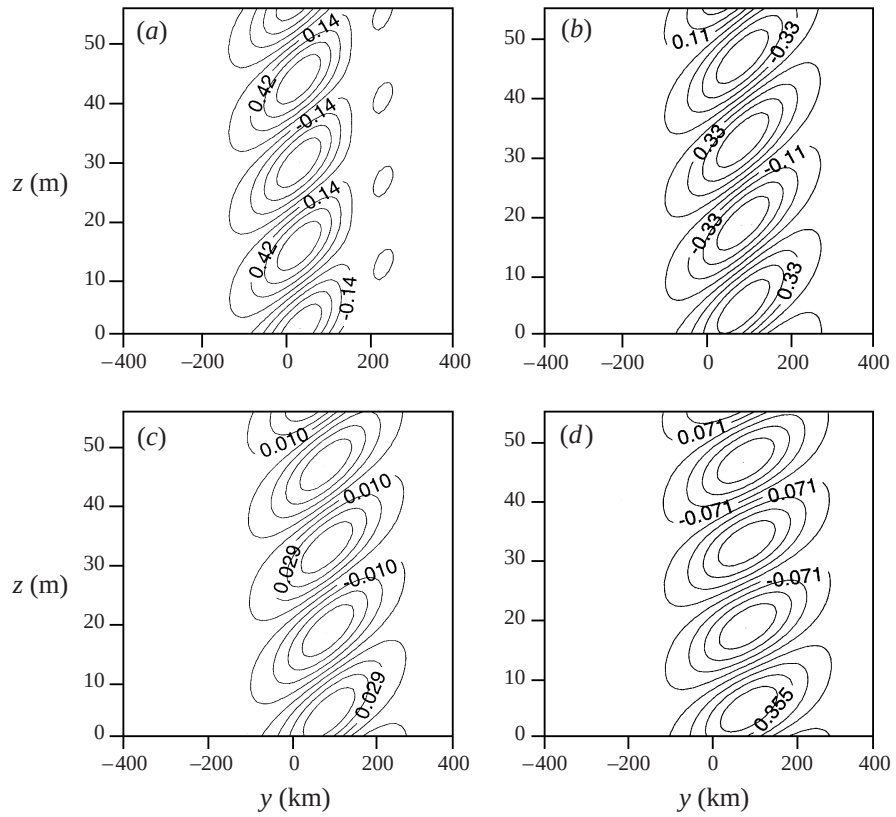

FIGURE 5. Most unstable double-diffusive–inertial mode with latitudinal shear for $\bar{S}_y = -2 \times 10^{-5}$ p.s.u. m^{-1}, $\bar{S}_z = 3 \times 10^{-2}$ p.s.u. m^{-1}, $\Lambda = 2 \times 10^{-6}$ s^{-1}, $G = 0$, $N = 0.02$ s^{-1}, (*a*) u' (cm s^{-1}), (*b*) v' (cm s^{-1}), (*c*) S' (p.s.u.), (*d*) T' (K).

shear production, denoted P; buoyant production, or transfer from mean potential energy, denoted B; viscous dissipation, denoted D; and northward flux divergence, denoted F. The plot clearly shows that, at these parameter values, the disturbance is extracting energy from both the mean shear and the mean stratification. Diffusive loss is comparable in magnitude to the shear production and buoyancy terms, and the flux term is also locally large, acting to redistribute energy from the centre to the periphery of the disturbance. With no mean shear the shear production term would be identically zero, but a small buoyancy effect remains even as the salinity gradients and the diffusion tend to zero, as a result of vertical advection of the mean density structure. For these parameters the residual buoyancy term is an order of magnitude smaller with no salinity gradient, for a given northward velocity amplitude. Thus double diffusion is the dominant, but not the only, process contributing to the buoyancy term B.

Figure 7 shows the spatial structure of a mode in the oscillatory regime, with parameters $\bar{S}_y = -5 \times 10^{-6}$ p.s.u. m^{-1}, $\bar{S}_z = 3 \times 10^{-2}$ p.s.u. m^{-1}, $\Lambda = 2 \times 10^{-6}$ s^{-1}, $N = 0.02$ s^{-1}. The growth rate in this case is $\lambda = (0.22 + 0.78\mathrm{i}) \times 10^{-6}$ s^{-1}, hence the structure is propagating vertically at a rate which is comparable to its linear growth rate. With a significant imaginary component to λ, it is no longer obvious from (2.7) and (2.8) what the slope of the layers will be, nor where the centre of the disturbance will be located. The most striking aspect of figure 7 is that

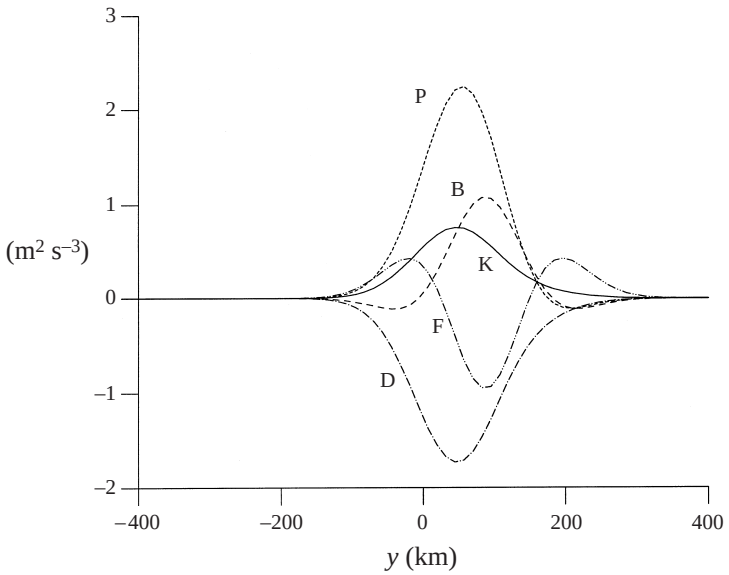

FIGURE 6. Terms in the vertically integrated kinetic energy equation (5.7) for the most unstable mode when $\bar{S}_y = -2 \times 10^{-5}$ p.s.u. m^{-1}, $\bar{S}_z = 3 \times 10^{-2}$ p.s.u. m^{-1}, $A = 2 \times 10^{-6}$ s^{-1}, $N = 0.02$ s^{-1}. K, rate of change of kinetic energy; P shear production; B, buoyancy; D, viscous dissipation; F, northward flux.

the slope of the thermohaline intrusions, although variable between T and S and variable in space, is predominantly of the wrong sign to promote instability by double diffusion, despite the fact that the salinity gradient is still quite large. Indeed, the growth rate in the oscillatory region actually decreases slightly with increasing salinity gradient. Investigation of the energy balance for this mode shows that the growth of the disturbance is driven by shear, with buoyancy effects an order of magnitude smaller. The disturbance to the temperature field is therefore produced largely by passive advection of the mean vertical stratification. Vertical advection gives rise to an antisymmetric system of temperature cells, and the sloping layers are the result of diffusion acting to reconnect diagonally adjacent cells.

5.2. *Variation with vertical salinity gradient*

In linearizing the governing equations we have neglected variation of the double-diffusive fluxes with the stability ratio $R_\rho = \alpha T_z / \delta S_z$. Such variations are known to be strong, with fluxes being strongly peaked for R_ρ close to 1 (Schmitt 1994). Since the stability ratio is related to the dimensionless vertical salinity gradient by by $R_\rho = 1 + (1 - \gamma)/\epsilon_z$, this would correspond to a variation of the diffusivity A with $\bar{S}_z$ in our problem, but since the form of the dependence is not well known, we prefer to vary $\bar{S}_z$ keeping A fixed and thus only consider the direct effect of variations in $\bar{S}_z$. Such variations turn out to be weak for ϵ_z in the realistic range from 0 to 1, or $\bar{S}_z$ in the range 0 to 0.1 p.s.u. m^{-1}. When double diffusion is the driving mechanism, increasing $\bar{S}_z$ from 0 to 0.1 p.s.u. m^{-1} results in a decrease in the growth rate by 25% to 50%. This is to be expected from the instability mechanism described earlier, as the instability is driven by the advection of mean salinity in the rising, warm, salty intrusions. As the vertical salinity gradient is increased, the along-layer salinity gradient in the rising layers, and hence the growth rate, is reduced, for a given layer slope. Note, however, that allowing A to vary with R_ρ could lead instead to an

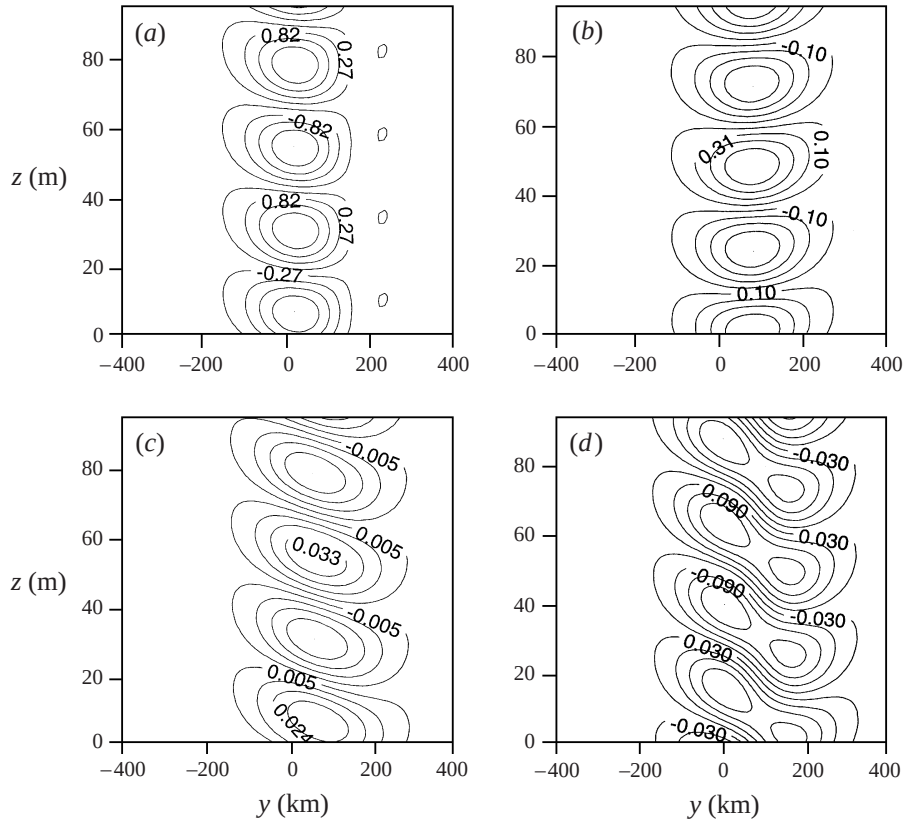

FIGURE 7. Most unstable double-diffusive–inertial mode in the oscillatory regime for $\bar{S}_y = -5 \times 10^{-6}$ p.s.u. m^{-1}, $\bar{S}_z = 3 \times 10^{-2}$ p.s.u. m^{-1}, $\Lambda = 2 \times 10^{-6}$ s^{-1}, $N = 0.02$ s^{-1}. (*a*) u' (cm s^{-1}), (*b*) v' (cm s^{-1}), (*c*) S' (p.s.u.), (*d*) T' (K).

increase in growth rate with increasing $\bar{S}_z$, since increasing $\bar{S}_z$ would bring R_ρ closer to 1, increasing the double-diffusive fluxes (Walsh & Ruddick 1995).

In the oscillatory band of viscous instability, the real and imaginary parts of the growth rates are enhanced by around 30% as $\bar{S}_z$ increases from 0 to 0.1 p.s.u. m^{-1}. This enhancement can be explained by the above argument, given that the slope of the thermohaline intrusions in this regime is opposite to that in the pure double-diffusion regime, as seen in figure 7. When inertial effects dominate the instability process the effect of $\bar{S}_z$ on the growth rate is negligible.

5.3. *Fluxes*

The potential of the instability modes described above to influence the larger-scale flow depends on the net transports of heat, salt and momentum which they produce. Of particular interest in the present context are cross-equatorial fluxes. All the linear components of the fluxes, such as $v'\bar{S}$, must have zero vertical average, since the solutions are sinusoidal in z. Hence we must look to the nonlinear components, such as $v'S'$, to determine the vertically averaged transports. In the constant-f case, as noted by McDougall (1985), the divergences of the nonlinear advective terms are zero, hence the nonlinear terms have no net effect on the mean salinity field, for example, although the components of the fluxes are not individually zero. Our solutions are

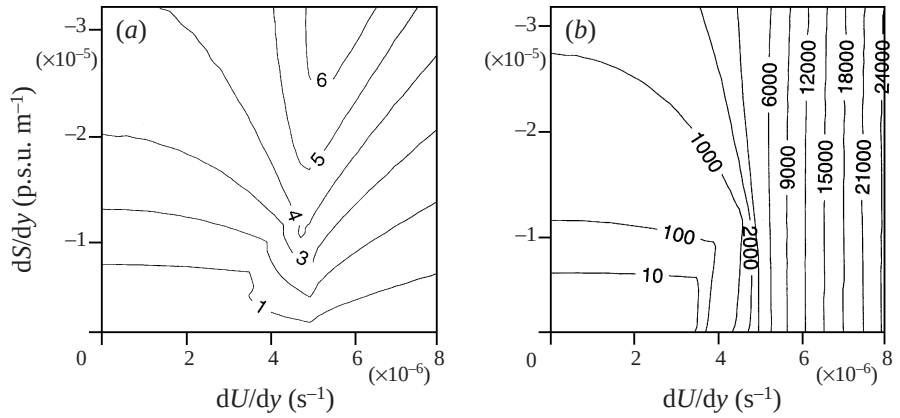

FIGURE 8. (*a*) Maximum vertically averaged northward salinity flux F_S in units of 10^{-4} p.s.u. m s^{-1} for the fastest growing linear mode as a function of Λ and $\bar{S}_y$, at $\bar{S}_z = 3 \times 10^{-2}$ p.s.u. m^{-1}, $N = 0.02$ s^{-1}, for a northward velocity amplitude of 1 cm s^{-1}. (*b*) Effective diffusivity $\kappa_{\text{eff}} = -F_S/\bar{S}_y$ in m^2 s^{-1} defined by setting the velocity amplitude to $L\lambda_r$ (see text).

trapped at the equator, hence the resulting fluxes vary with y and can therefore act to change the mean fields.

Since the linearly unstable solutions grow exponentially in time, linear theory is limited to predicting scaling behaviour, and to calculating how the fluxes in the linear solution vary with the input parameters. In order to calculate the variation of salinity fluxes, we arbitrarily choose to set the amplitude of the northward velocity perturbation to 1 cm s^{-1} (Banks & Richards 1998 argue that northward velocities of this magnitude are required for a nonlinear balance). Figure 8(*a*) shows the variation of the latitudinal maximum value, F_S, of the resulting northward salinity flux with $\bar{S}_y$ and Λ; other parameters are as used above ($\bar{S}_z = 3 \times 10^{-2}$ p.s.u. m^{-1}, $N = 0.02$ s^{-1}). We expect the northward salinity flux to increase with the northward salinity gradient $\bar{S}_y$, therefore it is sensible to consider the ratio $F_S/\bar{S}_y$. This ratio represents an effective diffusivity, but we are restricted by our inability to predict the absolute amplitude of the disturbance. One possible solution is to suggest a scaling for v' based on the predicted length and time scales of the fastest growing linear mode, since the linear solution has a well-defined latitudinal length scale $L = \sqrt{2}/\mathrm{Re}\,(C\beta)$ and a well-defined inverse time scale $\lambda_r = \mathrm{Re}\,(\lambda)$. We can then define an effective diffusivity κ_{eff} by taking the maximum salinity flux F_S for a velocity amplitude of $L\lambda_r$ and setting $\kappa_{\text{eff}} = -F_S/\bar{S}_y$. Interestingly this quantity, which is plotted in figure 8(*b*), shows a close resemblance in form to the real part of the growth rate shown in figure 3. Richards (1998) has suggested two separate forms κ_{DD} and κ_{II} for the lateral diffusivity due to equatorial interleaving driven by double diffusion and inertial instability respectively. These are given by

$$\kappa_{\text{DD}} = \left(\frac{N^3 A \epsilon_y}{16 \beta^2 \sigma^{1/2}} \right)^{1/2}, \tag{5.8}$$

$$\kappa_{\text{II}} = \frac{1}{\sigma} \left(\frac{N^6 A^3}{4\beta^4} \right)^{1/5}. \tag{5.9}$$

For large absolute values of salinity gradient $3 \times 10^{-4} > |\bar{S}_y| > 3 \times 10^{-5}$ p.s.u. m^{-1} (not

shown) and for $\Lambda = 0$ the dependence of κ_{DD} on $\bar{S}_y$ shows qualitative agreement with κ_{eff}, which increases by a factor of around 5 across this range. In the inertially unstable regime, however, κ_{II} does not increase with Λ. The increase of κ_{eff} with Λ found here reflects the fact that the growth rate λ approaches Λ for large shear. The increase of κ_{eff} is not unreasonable if faster linear growth leads to stronger cross-equatorial flow in the nonlinear regime, and hence larger tracer fluxes, for a given tracer gradient.

6. Effect of vertical shear

To consider the effect of vertical shear we revert to the general case given by equations (2.3) to (2.10). However we continue to make the hydrostatic assumption, which results in the equation for a in (2.4) being replaced by the simpler form given in (4.1). To gauge the effect of vertical shear we consider the equation for $\hat{v}$ with respect to the transformed vertical coordinate z^* (defined by (2.6)), which takes the form

$$a\hat{v}_{yy} + c'\hat{v} = 0, \tag{6.1}$$

where

$$c' = c - b_1 - \frac{b^2}{4a} = c_2 y^2 + c_1 y + c_0 \tag{6.2}$$

and c_0, c_1 and c_2 are constants given by

$$\left.\begin{aligned} c_0 &= -\frac{m^2}{N^2}\lambda\lambda_A\lambda_v\left(1 - \frac{A^2m^4\epsilon_y^2N^2}{4a\lambda\lambda_A\lambda_v} - \frac{\mathrm{i}v\beta Gm}{2\lambda\lambda_v^2}\right), \\ c_1 &= 2\Lambda\beta\frac{m^2}{N^2}\frac{\lambda\lambda_A}{\lambda_v}\left(1 - \frac{Am^2\epsilon_y G(\lambda+\lambda_v)}{4\Lambda a\lambda}\right), \\ c_2 &= -\left(\frac{m\beta}{N}\right)^2\frac{\lambda\lambda_A}{\lambda_v}\left(1 - \frac{G^2}{N^2}\frac{\lambda_A(\lambda+\lambda_v)^2}{4a\lambda\lambda_v}\right). \end{aligned}\right\} \tag{6.3}$$

The contribution due to vertical shear to the term c_2, which affects the meridional scale of the solutions, is thus G^2/N^2 multiplied by an order-one number. This contribution is therefore independent of the sign of G and is typically small in the equatorial thermocline outside strong jets such as the equatorial undercurrent. In the ideal fluid case this is the only effect of vertical shear, and for $G^2/N^2 > 1$ there are no equatorially trapped, unstable solutions to the linear, inviscid problem. A slightly weaker criterion applies if the horizontal component of the Earth's rotation vector is included (Hua *et al.* 1997).

The contribution due to vertical shear to c_1 is of order $Am^2\epsilon_y G/\lambda\Lambda$. If we suppose that a realistic value for A is around $10^{-5}\,\mathrm{m^2\,s^{-1}}$, and that the instability has scales of $m \approx 0.1\,\mathrm{m^{-1}}$ and $\lambda \approx 10^{-7}\,\mathrm{s^{-1}}$, then Am^2 is of order λ and the contribution is of order $\epsilon_y G/\Lambda$. This term affects the position of the axis of symmetry of solutions with respect to the equator, and the contribution occurs only as a result of interaction between vertical shear and horizontal salinity gradients. This contribution is also typically small except for large vertical shear.

The contribution to c_0 due to G is complex, tending to promote oscillatory instability. Assuming, as above, that $Am^2 = O(\lambda)$, and similarly that $vm^2 = O(\lambda)$, then the contribution is of order

$$\left(\frac{\beta G}{m\lambda^2 + m\epsilon_y^2N^2}\right). \tag{6.4}$$

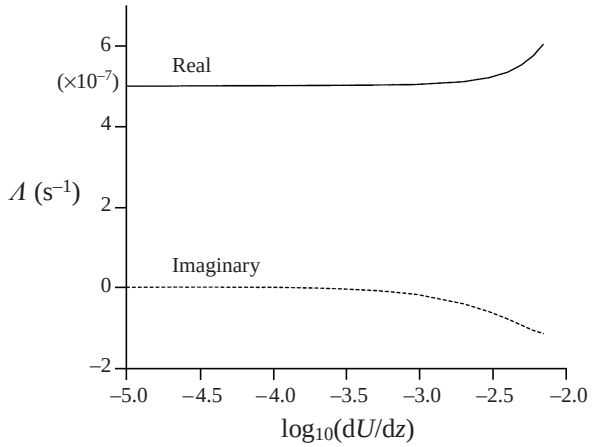

FIGURE 9. Real and imaginary parts of the growth rate of the most unstable mode as a function of $\log_{10}$ vertical shear in s^{-1}. $N = 0.02\,s^{-1}$, $\bar{S}_y = -2 \times 10^{-5}$ p.s.u. m^{-1}, $\bar{S}_z = 3 \times 10^{-2}$ p.s.u. m^{-1}, $\Lambda = 0$.

Taking $\beta \approx 10^{-11}\,m^{-1}\,s^{-1}$ and using the same scales for m and λ as above, we would expect significant modification for $|G| \geqslant 10^{-4}\,s^{-1}$. This contribution arises from advection of mean density and relies on the differential diffusion of momentum and density, and on the northward curvature of the density field, $\overline{\rho}_{yy}$. With constant vertical shear on the equatorial β-plane, $\overline{\rho}_y$ is proportional to y. Taking $\overline{\rho}_y$ to be constant would eliminate this complex behaviour, but would result in a vertical shear profile with a singularity at the equator.

The other two contribution terms, to c_2 and c_1, enter via b_1 and are due equally to advection of density, and to vertical advection of momentum, the term $w'G$ in (2.1).

6.1. *Results for non-zero G*

The above discussion suggests that vertical shear G is unlikely to affect the results significantly for $G^2 \ll N^2$. Note that the analysis of Hua *et al.* (1997) shows that the inviscid criterion for inertial instability triggered by purely vertical shear in the traditional approximation is $N^2/G^2 < 1$, but solutions are only equatorially trapped if $N^2/G^2 > 1$. Numerical solutions of the dispersion relation show little dependence on vertical shear for $G^2 \ll N^2$. Figure 9 is a plot of the growth rate of the most unstable mode for vertical shear G in the range $10^{-5} \leqslant G \leqslant 0.007\,s^{-1}$, when $N = 0.02\,s^{-1}$ and the salinity gradients take the values $\bar{S}_y = -2\times10^{-5}$ p.s.u. m^{-1}, $\bar{S}_z = 3\times10^{-2}$ p.s.u. m^{-1}. The growth rate changes by 20% across this range of shear, while the corresponding change in vertical wavenumber of the most unstable mode (not shown) is less than 10%. The most significant effect of vertical shear is the appearence of an oscillatory component of the growth rate. The spatial structure of the most unstable mode is shown in figure 10 for $G = 0.005\,s^{-1}$. The growth rate in this case is $(0.5-0.1i)\times10^{-6}\,s^{-1}$ and the most unstable vertical wavenumber is $0.305\,m^{-1}$. Vertical shear shifts the centre of the disturbance away from the equator and induces an asymmetry in the zonal jet structure compared with the solution with no mean shear in figure 4. The northward displacement y_0 of the maximum in the northward velocity field, as given in (2.9), is

$$y_0 = \frac{4a\lambda\lambda_v\Lambda - Am^2\lambda_v\epsilon_y G(\lambda+\lambda_v)}{4a\beta\lambda_v\lambda - \lambda_A\beta(G/N)^2(\lambda+\lambda_v)^2}.$$

Thus for $\Lambda = 0$ the sign of the displacement depends on the sign of G.

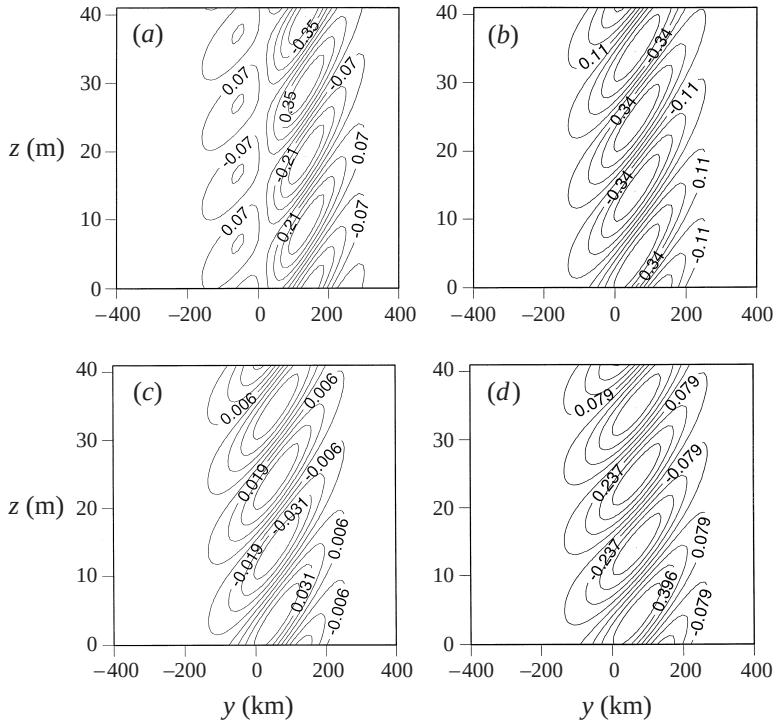

FIGURE 10. Most unstable double-diffusive–inertial mode with vertical shear for $G = 0.005\,\mathrm{s}^{-1}$, $N = 0.02\,\mathrm{s}^{-1}$, $\bar{S}_y = -2 \times 10^{-5}$ p.s.u. m^{-1}, $\bar{S}_z = 3 \times 10^{-2}$ p.s.u. m^{-1}, $\Lambda = 0$. (*a*) u' (cm s^{-1}), (*b*) v' (cm s^{-1}), (*c*) S' (p.s.u.), (*d*) T' (K).

When the absolute value of G is small, the maximum growth rate occurs at a finite wavenumber m_c. For large values of $|G|$, greater than about $10^{-3}\,\mathrm{s}^{-1}$ when $N = 0.02\,\mathrm{s}^{-1}$, the numerically determined growth rate may still have a local maximum at finite m, but increases as m becomes very small or very large. These 'small m' and 'large m' modes only become dominant at values of G which are rather large for the equatorial region as a whole, but could easily occur in regions of strong shear such as the edge of the equatorial undercurrent.

A typical example of a small-m mode is shown in figure 11, which is the fastest growing linear mode at $m = 0.025\,\mathrm{m}^{-1}$, with $G = 0.005\,\mathrm{s}^{-1}$, $N = 0.02\,\mathrm{s}^{-1}$, $\bar{S}_y = -2 \times 10^{-5}$ p.s.u. m^{-1}, $\bar{S}_z = 3 \times 10^{-2}$ p.s.u. m^{-1}. These modes are characterized by rapid rates of oscillation, the growth rate λ in this particular case being $(1.0+4.3\mathrm{i}) \times 10^{-6}\,\mathrm{s}^{-1}$. With both $\bar{S}_z$ and $\bar{S}_y$ set to zero, but other parameters unaltered, the growth rate is the same to 3 decimal places, indicating that the instability is driven by the mean vertical shear and not by double diffusion. However, as discussed by Hua *et al.* (1997), there are no equatorially trapped, linearly unstable modes driven purely by vertical shear. Hence these must be viscous modes similar to those discussed by McIntyre (1970) since, in our parameterization, setting both $\bar{S}_z$ and $\bar{S}_y$ to zero corresponds to setting diffusion to zero with finite viscosity, the limit of large Prandtl number. The temperature and salinity perturbations seen in figure 11 are therefore largely driven by advection, with double diffusion acting to reconnect diagonally adjacent cells of the same sign.

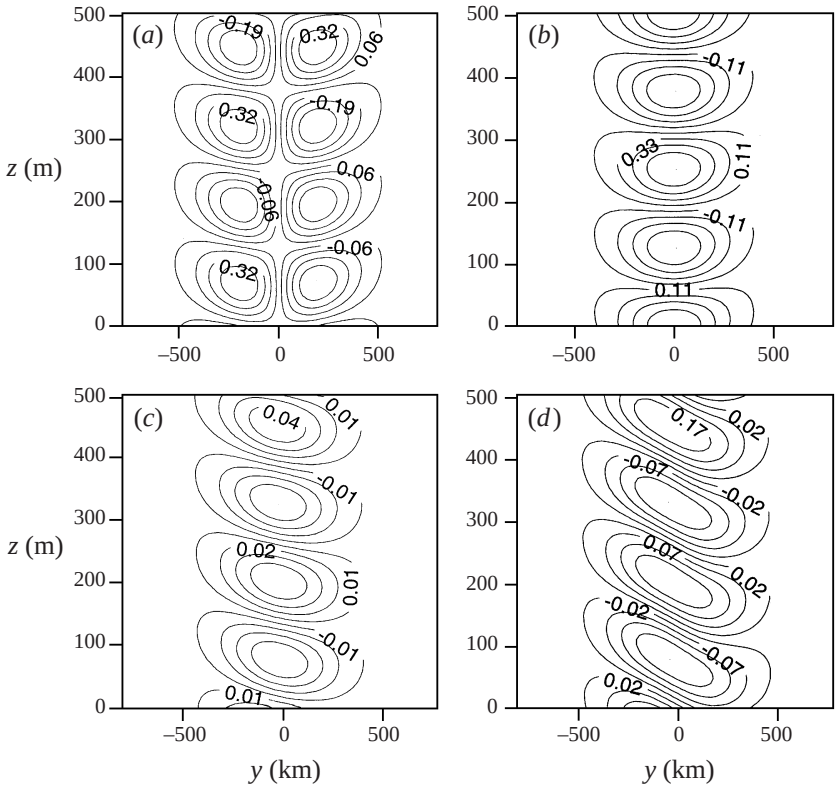

FIGURE 11. 'Small m' vertical shear double-diffusive-inertial mode for $m = 0.025\,\mathrm{m}^{-1}$, $G = 0.005$ s^{-1}, $N = 0.02\,\mathrm{s}^{-1}$, $\bar{S}_y = -2 \times 10^{-5}$ p.s.u. m^{-1}, $\bar{S}_z = 3 \times 10^{-2}$ p.s.u. m^{-1}, $\Lambda = 0$. (*a*) u' ($\mathrm{cm\,s}^{-1}$), (*b*) v' ($\mathrm{cm\,s}^{-1}$), (*c*) S' (p.s.u.), (*d*) T' (K).

The increase in growth rate which occurs for large m when $|G|$ is large appears to be related to singular behaviour of the equatorial offset y_0 (2.9). y_0 can become large if G^2/N^2 is close to 1, or for more moderate values of G/N if m is large. These large-m solutions therefore appear to be essentially an artefact of the model, since their growth rates do not become dominant until the associated equatorial offset has become unphysically large, invalidating the assumptions inherent in the β-plane approximation.

Singular behaviour of the governing linear equations has been shown to exist in a system similar to ours but without double diffusion by McIntyre (1970). The singularity is manifested in the discrepancy between the solution to the ideal problem, and the solution to the diffusive problem in the limit in which the viscosity and diffusivity are reduced to zero while their ratio (the Prandtl number) is kept constant. With double diffusion and large vertical shear, we find that even when the viscosity is kept constant, there is a discrepancy between the solution for small salinity gradients and the solution for zero salinity gradient. For instance at $G = 0.005\,\mathrm{s}^{-1}$, $m = 0.3\,\mathrm{m}^{-1}$, and other parameters as used above, but with zero mean salinity gradient, we find no instability. This corresponds to zero diffusivity in our system. However for an extremely small value of $\bar{S}_y = -1 \times 10^{-10}$ we find significant growth rates of order $10^{-7}\,\mathrm{s}^{-1}$, again associated with unphysical values of y_0. This discrepancy, like the small- and large-m modes, only appears for very large values of G, but we note that

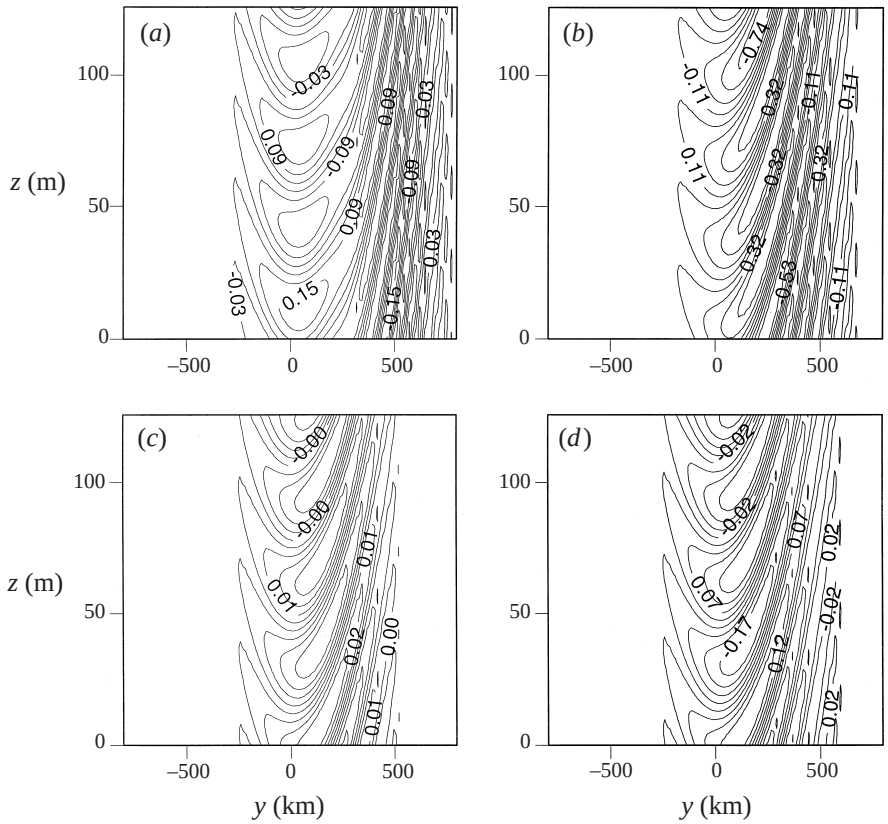

FIGURE 12. Strong vertical shear double-diffusive–inertial mode for $m = 0.1\,\mathrm{m}^{-1}$, $G = N = 0.02\,\mathrm{s}^{-1}$, $\bar{S}_y = -2 \times 10^{-5}\,\mathrm{p.s.u.\,m}^{-1}$, $\bar{S}_z = 3 \times 10^{-2}\,\mathrm{p.s.u.\,m}^{-1}$, $\Lambda = 0$. (*a*) u' ($\mathrm{cm\,s}^{-1}$), (*b*) v' ($\mathrm{cm\,s}^{-1}$), (*c*) S' (p.s.u.), (*d*) T' (K).

problems may occur when the diffusivity is small, since this corresponds to the limit of large m, if we take the diffusivity to define the vertical scale.

These singularities effectively preclude the possibility of obtaining solutions for all values of vertical shear and salinity gradient with the current solution technique. A more complete investigation may require spherical coordinates and a more robust numerical method. However solutions can be obtained even for $G/N = 1$. Note that G^2/N^2 is an inverse Richardson number and hence turbulent mixing would be expected to dominate double-diffusive mixing for $G > 2N$. An example solution for $G/N = 1$ is shown in figure 12 for $m = 0.1\,\mathrm{m}^{-1}$, with $G = N = 0.02\,\mathrm{s}^{-1}$, $\bar{S}_y = -2 \times 10^{-5}\,\mathrm{p.s.u.\,m}^{-1}$, $\bar{S}_z = 3 \times 10^{-2}\,\mathrm{p.s.u.\,m}^{-1}$, the growth rate λ in this case being $(1.9 - 2.0\mathrm{i}) \times 10^{-6}\,\mathrm{s}^{-1}$. For these values of mean gradients, the largest growth rates occur for unphysically large and small wavenumber m. The solution shown corresponds to the most unstable mode at $m = 0.1\,\mathrm{m}^{-1}$ for which the equatorial offset $y_0 < 400\,\mathrm{km}$. Unphysical, non-equatorially trapped modes have therefore been excluded. The strong curvature of the intrusive layers visible in the figure almost exactly matches the curvature of the background density field implied by specifying a fixed vertical shear on a β-plane. The slope of the layers across isopycnals is relatively small, and the instability is driven largely by shear. As expected from our earlier analysis, the sign of the meridional displacement y_0 depends on the sign of $\bar{S}_y G$.

Changing the sign of G reverses the meridional curvature. The real part of the growth rate is unaffected by the sign of G and $\bar{S}_y$, as would be expected from inspection of the dispersion relation (2.10) in the case $\Lambda = 0$.

7. Non-hydrostatic effects

The effect of the hydrostatic assumption on the solution is to change the coefficient a of $\hat{v}_{yy}$ in (2.3) from the value given for the general solution in (2.4) to the simpler form given in (4.1). The difference between the two is the additional term

$$\frac{\lambda\lambda_A\lambda_v}{N^2}, \tag{7.1}$$

which is of order λ^2/N^2, relative to a. Since the largest growth rates for realistic parameters are typically around (10 days)$^{-1}$ the relative error on ignoring this correction is around 10^{-8} if $N^2 \approx 10^{-4}\,\mathrm{s}^{-2}$. Given the high order of the dispersion relation, the change in λ could be greater, but for all of the solutions plotted in figures 4, 5, 7, 10 and 11 the calculated growth rates were unaffected by the hydrostatic approximation to 5 significant figures. For sufficiently weak stratification, if $N^2 \ll \lambda^2$, the non-hydrostatic contribution will dominate.

8. Discussion and conclusions

We have investigated the linear stability of a zonally symmetric salinity front at the equator with horizontal and vertical shear. The most unstable zonally symmetric perturbations can be driven either by double diffusion or by inertial instability of the lateral shear. In a certain parameter regime strong interaction can occur between the two processes. Outside this region, meridional shear is found to enhance double-diffusive interleaving motion even for values of shear well below the cutoff for inertial instability. When double-diffusive driving is weak, relative to inertial driving, the growth can be oscillatory, in which case the mechanism is the viscous-diffusive instability found by McIntyre (1970) which relies on the differential diffusion of density and momentum (non-unit Prandtl number). In the latter case interleaving layers can slope downwards towards the fresh side of the front in the fingering regime, inhibiting their own growth.

Banks & Richards (1998) found average northward salinity gradients in the western equatorial Pacific of around -2×10^{-6} p.s.u. m^{-1} and values of N around $0.02\,\mathrm{s}^{-1}$. With the diffusion parameters used here, these values would indicate that the dominant primary instability process is inertial, rather than double-diffusive, instability. However, double-diffusive flux parameterizations are uncertain; Walsh & Ruddick (1995) found that even a weak dependence of the fluxes on the density ratio can significantly affect growth rates. Wave–convection coupling has also been found to significantly increase double-diffusive fluxes in the diffusive regime (Hughes & Nokes 1995). Since the double-diffusive interleaving instability acts to reduce the mean salinity gradient, it is also plausible that observed mean gradients in regions of fully developed interleaving may be lower than is relevant to a linear stability analysis. Double-diffusive interleaving is also enhanced by along-front variation (see below).

Clearly the use of a single constant value for the mean velocity shear is a gross approximation for the complex equatorial current system, but the range of values of shear in which double diffusion and inertial instability interact in the present model is reasonable; between 10 and 100 cm s^{-1} per degree of latitude. With diffusion, we find

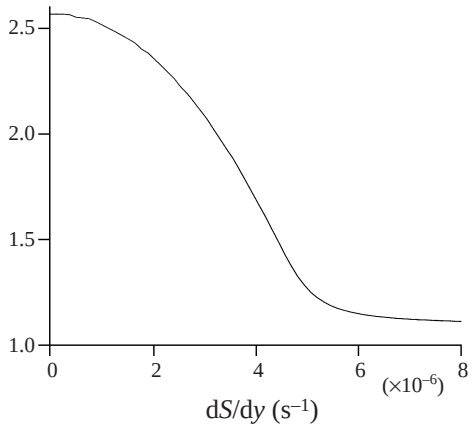

FIGURE 13. Variation of the ratio of averaged temperature to density perturbations in density units for $\bar{S}_y = -2 \times 10^{-5}$ p.s.u. m^{-1}, $\bar{S}_z = 3 \times 10^{-2}$ p.s.u. m^{-1}, $N = 0.02\,\mathrm{s}^{-1}$.

that vertical shear can also drive equatorially trapped modes, but only if the strength of the vertical shear is comparable to the buoyancy frequency.

The above discussion suggests that both double-diffusive and inertial instability may be important in the formation of observed interleaving layers in the equatorial Pacific and raises the question of how to distinguish between double-diffusive and inertially driven modes in practice. Double diffusion can act to enhance or to inhibit the growth of inertial instability modes depending on the strength of the salinity gradient. With latitudinal mean shear the centre of the disturbance is offset from the equator and the growth can be oscillatory, but these characteristics are not sufficient to indicate that shear is a driving mechanism, since double-diffusive interleaving with along-front variation can have the same characteristics (Richards 1991). The most unstable wavenumber is similar for shear-driven and double-diffusively driven disturbances, so observed vertical wavenumbers are not very helpful in distinguishing between the two driving mechanisms. For double-diffusive interleaving with constant Coriolis parameter f, McDougall (1985) calculates various 'observable' ratios of disturbance quantities. These ratios are meaningful if the relevant quantities are in phase. When f varies with latitude y, different disturbance quantities are not generally in phase. Of particular significance is the fact that the direction of the disturbance velocity is not constant. In McDougall's problem the disturbance velocity is always directed along the interleaving layers, so that all nonlinear terms such as $\boldsymbol{u}' \cdot \nabla S'$ are zero. This means that a linear solution is also technically a finite-amplitude solution. In our case the nonlinear terms will not, in general, be zero and ratios of disturbance quantities calculated locally may not always be finite. McDougall calculates ratios of velocity component amplitudes, velocity to buoyancy perturbation amplitudes, along-leaf temperature and salinity gradients and temperature and salinity disturbance amplitudes. For the double-diffusive–inertial modes found above, we can calculate these ratios after averaging in y and z. Amongst the ratios calculated by McDougall, the ratio of perturbation temperature to salinity amplitudes shows the most marked variation with shear and therefore offers the greatest possibility of distinguishing between shear and double-diffusively driven instabilities. This ratio is plotted in figure 13 as a function of latitudinal shear for $\bar{S}_y = -2 \times 10^{-5}$ p.s.u. m^{-1}, $\bar{S}_z = 3 \times 10^{-2}$ p.s.u. m^{-1} and $N = 0.02\,\mathrm{s}^{-1}$. When the instability is driven by shear, the thermohaline perturbations are produced essentially by horizontal advection

and hence the ratio is close to one. When double-diffusive fingering is dominant, the greater diffusion of salinity reduces the salinity perturbation relative to the temperature perturbation. The value of the ratio also varies with salinity gradient, in contrast with McDougall's result. This discrepancy may be due to our assumption of two-dimensionality. In the absence of dissipation the most unstable inertial instability modes are zonally symmetric (Dunkerton 1983). The results of Richards (1991) show that the most unstable linear double-diffusive equatorial interleaving modes have non-zero along-front wavenumber k for values of $|\epsilon_y|$ below about 10^{-3}. For the parameters used above this corresponds to values of $|\bar{S}_y|$ below about 10^{-4} p.s.u. m^{-1}. For $\epsilon_y = -3 \times 10^{-4}$ Richards (1991) found that the maximum growth rate was approximately 2.5 times greater than the most unstable $k = 0$ value. Hence the present theory may underestimate the importance of double diffusion for small values of latitudinal salinity gradient. With along-front variation as well as lateral shear the linear eigenfunctions can only be found by approximate methods (Clarke & Haynes 1996).

An often-cited characteristic property of double-diffusive intrusions is their upward slope across isopycnal surfaces. Woods *et al.* (1986) showed that three-dimensional isopycnal advection can also create intrusions which are inclined to isopycnals, thus highlighting the danger of interpreting two-dimensional observations in terms of purely two-dimensional mechanisms. May & Kelley (1997) have shown that, even in two dimensions, double-diffusive intrusions driven by salt fingering in the presence of baroclinic shear can slope downwards across isopycnals if they rise across geopotential surfaces. Interleaving motion was found to be enhanced if isopycnals rose towards the fresh side of the front. The present results show that inertial instability can lead to thermohaline intrusions which slope downwards across both isopycnals and geopotential surfaces, inhibiting their own growth, even in the salt fingering regime with significant mean thermohaline gradients. It is also important to note that any thermohaline intrusion with temperature and salinity perturbations roughly in phase, such as the modes found above, would lead to a pattern of vertical thermohaline gradients alternating in the vertical between fingering and diffusive double-diffusion regimes, if the form of the solution remained self-similar to sufficiently large amplitude. The present results cannot be applied to finite-amplitude intrusions since the parameterization of vertical diffusivity becomes inadequate when inversions occur in the vertical thermohaline gradients (effectively γ varies with vertical thermohaline gradients). The behaviour of the system at finite amplitude and the relative effects of double diffusion and shear on fully developed intrusions are currently being studied by numerical simulation and will form the basis of a subsequent paper.

This work was supported by UK Natural Environment Research Council Grant GR3/10502.

REFERENCES

Banks, H. T. & Richards, K. J. 1998 Intrusions in the western equatorial Pacific. Submitted to *J. Geophys. Res.*

Clarke, P. D. & Haynes, P. H. 1996 Inertial instability on an asymmetric low-latitude flow. *Q. J. R. Met. Soc.* **122**, 151–182.

Dunkerton, T. J. 1981 On the inertial stability of the middle atmosphere. *J. Atmos. Sci.* **38**, 2354–2364.

Dunkerton, T. J. 1983 A nonsymmetric equatorial inertial instability. *J. Atmos. Sci.* **40**, 807–813.

Hua, B. L., Moore, D. W. & Le Gentil, S. 1997 Inertial nonlinear equilibration of equatorial flows. *J. Fluid Mech.* **331**, 345–371.

Hughes, G. O. & Nokes, R. I. 1995 Wave convection coupling in multi-component convection: an experimental study. In *Double Diffusive Convection* (ed. A. Brandt & H. J. S. Fernando). American Geophys. Union.

Jeffreys, H. & Jeffreys, B. 1956 *Methods of Mathematical Physics.* Cambridge University Press.

Kunze, E. 1990 The evolution of salt fingers in inertial wave shear. *J. Mar. Res.* **48**, 471–504.

May, B. D. & Kelley, D. E. 1997 Effect of baroclinicity on double-diffusive interleaving. *J. Phys. Oceanogr.* **27**, 1997–2008.

McDougall, T. J. 1985 Double-diffusive interleaving. Parts I and II. *J. Phys. Oceanogr.* **15**, 1532–1555.

McIntyre, M. E. 1970 Diffusive destabilization of the baroclinic circular vortex. *Geophys. Fluid Dyn.* **1**, 19–57.

McPhaden, M. J. 1985 Fine-structure variability observed in CTD measurements from the central equatorial Pacific. *J. Geophys. Res.* **90**, 11726–11740.

Neelin, J. D., Latif, M., Allaart, M. A. F., Cane, M. A., Cubash, U., Gates, W. L., Gent, P. R., Ghil, M., Gordon, C., Lau, N. C., Mechoso, C. R., Meehl, G. A., Oberhuber, J. M., Philander, S. G. H., Schopf, P. S., Sperber, K. R., Sterl, A., Tokioka, T., Tribbia, J. & Zebiak, S. E. 1992 Tropical air-sea interaction in general circulation models. *Climate Dyn.* **7**, 73–104.

Rayleigh, Lord 1916 On the dynamics of revolving fluids. *Proc. R. Soc. Lond.* A **93**, 447–453.

Richards, K. J. 1991 Double-diffusive interleaving at the equator. *J. Phys. Oceanogr.* **21**, 933–938.

Richards, K. J. 1998 Interleaving at the equator. *Proc. NATO ASI on Ocean Modelling and Parameterization* (ed. E. P. Chassignet & J. Verron), Series C, Vol. 516, pp. 235–252. Kluwer.

Richards, K. J. & Pollard, R. T. 1991 Structure of the upper ocean in the western equatorial Pacific. *Nature* **350**, 48.

Ruddick, B. R. 1985 Momentum transport in thermohaline staircases. *J. Geophys. Res.* **90**, 895–902.

Ruddick, B. R., Griffiths, R. W. & Symonds, G. 1989 Frictional stress at a sheared double-diffusive interface. *J. Geophys. Res.* **94**, 18161–18173.

Ruddick, B. R. & Hebert, D. 1988 The mixing of meddy 'sharon'. In *Small Scale Turbulence and Mixing in the Ocean* (ed. J. Nihoul & B. Jamart), pp. 249–261. Elsevier.

Schmitt, R. W. 1994 Double diffusion in oceanography. *Ann. Rev. Fluid Mech.* **26**, 255–285.

Stern, M. E. 1967 Lateral mixing of water masses. *Deep-Sea Res.* **14**, 747–753.

Toole, J. M. 1981 Anomalous characteristics of equatorial thermocline finestructure. *J. Phys. Oceanogr.* **11**, 871–876.

Toole, J. M. & Georgi, D. T. 1981 On the dynamics and effects of double-diffusively driven intrusions. *Prog. Oceanogr.* **10**, 123–145.

Turner, J. S. 1967 Salt fingers across a density interface. *Deep-Sea Res.* **14**, 599–611.

Walsh, D. & Ruddick, B. 1995 Double-diffusively driven intrusions: the influence of non-constant diffusivities. *J. Phys. Oceanogr.* **25**, 348–358.

Woods, J. D., Onken, R. & Fischer, J. 1986 Thermohaline intrusions created isopycnally at oceanic fronts are inclined to isopycnals. *Nature* **322**, 446–448.

Zhang, J., Schmitt, R. W. & Huang, R. X. 1998 Sensitivity of the GFDL modular ocean model to parameterization of double-diffusive processes. *J. Phys. Oceanogr.* **28**, 589–605.